# Single-Molecule Microscopy on Model Membranes Reveals Anomalous Diffusion

G. J. Schütz, H. Schindler, and Th. Schmidt
Institute for Biophysics, University of Linz, 4040 Linz, Austria

ABSTRACT The lateral mobility of lipids in phospholipid membranes has attracted numerous experimental and theoretical studies, inspired by the model of Singer and Nicholson (1972. *Science.* 175:720–731) and the theoretical description by Saffman and Delbrück (1975. *Proc. Natl. Acad. Sci. USA.* 72:3111–3113). Fluorescence recovery after photobleaching (FRAP) is used as the standard experimental technique for the study of lateral mobility, yielding an ensemble-averaged diffusion constant. Single-particle tracking (SPT) and the recently developed single-molecule imaging techniques now give access to data on individual displacements of molecules, which can be used for characterization of the mobility in a membrane. Here we present a new type of analysis for tracking data by making use of the probability distribution of square displacements. The potential of this new type of analysis is shown for single-molecule imaging, which was employed to follow the motion of individual fluorescence-labeled lipids in two systems: a fluid-supported phospholipid membrane and a solid polymer-stabilized phospholipid monolayer. In the fluid membrane, a high-mobility component characterized by a diffusion constant of 4.4 $\mu m^2/s$ and a low-mobility component characterized by a diffusion constant of 0.07 $\mu m^2/s$ were identified. It is proposed that the latter characterizes the so-called immobile fraction often found in FRAP experiments. In the polymer-stabilized system, diffusion restricted to corrals of 140 nm was directly visualized. Both examples show the potentials of such detailed analysis in combination with single-molecule techniques: with minimal interference with the native structure, inhomogeneities of membrane mobility can be resolved with a spatial resolution of 100 nm, well below the diffraction limit.

## INTRODUCTION

Since its publication, the fluid mosaic model by Singer and Nicholson (1972) has set the framework for the interpretation of lateral diffusion on cell membranes. The mobility of lipids and proteins has been found to be a major principle controlling the structure and function of biomembranes (for reviews see Edidin, 1992; Zhang et al., 1993), such as large-scale aggregation (Gross and Webb, 1986) and diffusion-controlled biomolecular reactions (Peters, 1988). Because of its enormous structural and functional importance, the mobility of lipids and membrane-bound proteins embedded in model systems and cell membranes has been extensively studied experimentally (Gross and Webb, 1986; Edidin et al., 1991; Kusumi et al., 1993) and theoretically (Saffman and Delbrück, 1975; Saxton, 1993). Experimentally, the technique of fluorescence recovery after photobleaching (FRAP) has been commonly employed (Axelrod et al., 1976; Sheetz et al., 1980; Tamm, 1988; Tocanne, 1992; Kubitschek et al., 1994). In FRAP experiments, fluorescence-marked molecules are irreversibly photobleached by a short, intense laser flash focused to a micrometer size, and subsequently the recovery of the fluorescence signal due to diffusion of unbleached molecules into the bleached area is detected. The data are generally analyzed according to Brownian motion, yielding a value for the ensemble-averaged lateral diffusion constant. For most systems, an incomplete recovery of 70–95% (Tamm, 1988; Huang et al., 1992; Kalb et al., 1992; Kubitschek et al., 1994) has been observed and interpreted with a two-component model including a mobile and an immobile fraction of the species studied.

Complementary to FRAP, single-particle tracking (SPT) experiments have been developed that allow for observation of individual proteins (Ghosh and Webb, 1994; Anderson et al., 1992) or lipids (Lee et al., 1991) in biological membranes. In SPT, molecules are linked to either a highly fluorescent particle (Ghosh and Webb, 1994) or a nanometer-sized gold probe (Geerts et al., 1987), and the trajectory of the molecule is directly visualized by a video-enhanced imaging system. Very recently, several groups have succeeded in pushing the label size to the ultimate limit: a single fluorophore (Funatsu et al., 1995; Sase et al., 1995; Schmidt et al., 1996). The latter experiments have revealed local inhomogeneities and diffusion constants in supported phospholipid membranes on the basis of trajectories of individual fluorescence-labeled lipids.

Until now, most data obtained from SPT and single-molecule imaging experiments were analyzed in terms of mean square displacements (Gross and Webb, 1986; Anderson et al., 1992; Kusumi et al., 1993; Schmidt et al., 1995). However, tracking data give access not only to the mean, but to the full probability distribution of square displacements. A more detailed analysis would greatly increase the information of mobility studies, providing better insight into recent models of mobility in membranes. These models introduce more complex behaviors, including directional flow, lateral heterogeneities, and lateral constraints for diffusion (Edidin et al., 1991; Sako and Kusumi, 1995; Feder

*Received for publication 15 October 1996 and in final form 8 May 1997.*
Address reprint requests to Dr. Thomas Schmidt, Institute for Biophysics, University of Linz, 4040 Linz, Austria. Tel.: +43-732-2468-9265; Fax: +43-732-2468-822; E-mail: thomas.schmidt@jk.uni-linz.ac.at.
© 1997 by the Biophysical Society
0006-3495/97/08/1073/08 $2.00

et al., 1996; for a review see Jacobson et al., 1995); new SPT algorithms were introduced to differentiate between them (Kusumi et al., 1993; Quian et al., 1991; Saxton, 1993, 1994; Simson et al., 1995). In particular, the nanometer-scale precision of SPT experiments (Gelles et al., 1998; Kusumi et al., 1993) and a precision of tens of nanometers of single-molecule experiments (Schmidt et al., 1995) give these techniques the potential to be used to study inhomogeneities and lateral confinements for diffusion on a subwavelength scale.

We present here a different approach to analyzing the mobilities of individual molecules based on the probability distribution of individual displacements and apply this analysis to studies of the mobility of lipids in phospholipid membranes. Data were obtained from trajectories of individual lipids, each labeled by a single fluorophore, embedded in two different membranes: a fluid supported phospholipid membrane resembling free diffusional motion, and a solid polymer-stabilized phospholipid monolayer (Kowack and Helm, 1995) showing constrained diffusion. The high positional accuracy of ~50 nm and the high temporal resolution of 3.2 ms of our setup for single-molecule imaging make it possible to study mobilities on a subwavelength scale using a conventional optical system (Schmidt et al., 1995). In both membranes, a biphasic behavior of the diffusion is observed. Unrestricted diffusion with a diffusion constant of 4.4 $\mu m^2/s$ for a fast and 0.07 $\mu m^2/s$ for a slow mobility component is found in the fluid system. In addition, lateral constraints, typically 130 nm in size, were found at time scales below 100 ms. The solid system exhibits restricted diffusion, with a characteristic corral size of 140 nm.

## MATERIALS AND METHODS

### Sample preparation

#### *Supported phospholipid membranes*

Supported phospholipid membranes of 1-palmitoyl-2-oleoyl-*sn*-glycero-3-phosphocholin (POPC) (Avanti Polar Lipids, Alabaster, AL) were deposited on glass substrates by the Langmuir-Blodgett technique. Lipids were spread from chloroform at the air/buffer (100 mM NaCl, 10 mM $NaH_2PO_4$, pH 7.5) interface in a monolayer trough (Mayer Feintechnik, Göttingen, Germany) at room temperature. First a POPC monolayer was transferred vertically from the air/buffer interface onto a clean glass slide at a constant surface pressure of 32 mN/m. Subsequently, the monolayer-coated substrate was horizontally brought into contact with the second monolayer compressed to 32 mN/m, containing POPC and small amounts ($10^{-9}$ mol/mol) of *N*-(6-tetramethylrhodaminethiocarbamoyl)-1,2-dihexadecanoyl-*sn*-glycero-3-phosphoethanolamine, triethylammonium salt (TRITC-DHPE) (T-1391; Molecular Probes, Eugene, OR), equivalent to a surface density of $<0.01\ \mu m^{-2}$. The lipid bilayer on the substrate was pushed through the interface and clamped under water to an open quartz cell (136QS; Hellma, Müllheim, Germany). This cell was mounted on the microscope stage. The POPC membrane is known to be in the fluid state for the applied conditions (Tamm, 1988).

#### *Polymer-stabilized phospholipid monolayers*

Polymer-stabilized monolayers were obtained by deposition of a monolayer of 1,2-dimyristoyl-*sn*-glycero-3-phosphocholin (DMPC) (Sigma, Vienna, Austria), compressed to 32 mN/m, onto glass substrates. Subsequently, the hydrophobic substrate was brought into contact with a poly(methacrylate) (PMA) monolayer spread and compressed to 20 mN/m (the PMA was a kind gift of C. Helm, University of Mainz, Mainz, Germany). The latter contained 5% (w/w) POPC with small amounts of TRITC-DHPE ($6 \times 10^{-7}$ mol/(mol POPC)). The surface density of fluorescence-labeled lipid was less than 0.01 $\mu m^{-2}$. The PMA used had been derivatized with a hydrophilic and a hydrophobic substituent (Kowack and Helm, 1995). No large-scale lateral diffusion of the labeled molecules has been observed for the conditions employed (Kowack and Helm, 1995).

### Apparatus and data acquisition

The apparatus, data acquisition, and automatic data analysis system were used as previously described in detail (Schmidt et al., 1995). In brief, samples were illuminated by 528-nm circular polarized light from an $Ar^+$ laser (C306; Coherent, Santa Clara, CA) using a 100× objective (Plan-Neofluar, NA 1.3; Zeiss, Oberkochen, Germany) in an epifluorescence microscope (Axiovert 135TV; Zeiss). For experiments on the POPC membrane, illumination times were set to 5 ms and the illumination intensity to $25 \pm 6\ kW/cm^2$. Experiments on the polymer-stabilized monolayers were performed with an illumination time of 1 ms and an illumination intensity of $50 \pm 12\ kW/cm^2$. Rayleigh and Raman scattered light was effectively blocked by appropriate filter combinations (515DRLPEXT02 dichroic, 570DF70 block, Omega, Brattleboro, VT; OG550 low-pass, Schott, Mainz, Germany). Images were obtained by a liquid-nitrogen-cooled slow-scan CCD camera system (AT200, Photometrix, Tucson, AR, equipped with a TK512CB-chip, Tektronix) and stored on a PC. The delay between two consecutive observations was set to 15, 35, 75, and 155 ms for POPC membranes, and to 2.2 ms for the polymer-stabilized monolayers, respectively. The reduction of the illumination time for experiments on the PMA-stabilized monolayers allowed us to observe longer trajectories of individual molecules before photobleaching occurred. Up to 12 and 42 consecutive observations were obtained for the two systems, respectively. After 42 exposures the PMA-stabilized membranes were laterally shifted by 10 $\mu m$ with a motorized scanning stage, with a step size of 250 nm (SMS-3; OWIS, Staufen, Germany). In this way, data from multiple sample positions were collected. An automatic analysis program (Schmidt et al., 1995) determined the position of each fluorescence-labeled molecule with an accuracy of 54 nm by fitting the single-molecule fluorescence image to a two-dimensional Gaussian surface. The photon counts were determined to a precision of 20% (Schmidt et al., 1996). A Vogel algorithm was used to correlate the images of identical molecules in subsequent observations, from which the respective single molecule trajectories were reconstructed (Schmidt et al., 1995).

### Positional accuracy

The ratio of the fluorescence signal $F$ to the background noise $\sigma_B$ (= 6 counts) (Schmidt et al., 1996) determines the positional accuracy of the apparatus, $\sigma_r$ (Bobroff, 1986). $\sigma_r$ is defined as the standard deviation of the detected position $\tilde{r}$ from the true position. To quantify the positional accuracy, Monte Carlo experiments using the program MATLAB (MathWorks, Natick, MA) were performed. Images were generated from an immobile point source, randomly emitting 150 photons within 5 ms. The probability of detection of a photon in a particular pixel was given by a two-dimensional Gaussian distribution with a width of 1.6 pixels (full-width at half-maximum), specifying the point-spread function of the microscope. Background noise ($\sigma_B$ = 6 counts) was added to the image. In this way, 1000 images were generated with random variation of the position of the point source with regard to the pixel array. These images were subsequently analyzed by using the automatic detection and analysis program, yielding a mean positional deviation of $\sigma_r$ = 54 nm in each dimension. The value of $\sigma_r$ in two dimensions leads to an uncertainty in the determination of displacements of $\sqrt{4\sigma_r^2}$ = 108 nm.

Experiments on immobilized, highly fluorescent latex beads (30 nm, L-5271; Molecular Probes, Eugene, OR) performed on a time scale of 100 s yielded positional deviations of 16 nm. The decreased uncertainty is accounted for by the increased signal-to-background ratio obtained in bead compared to single fluorophore experiments (Bobroff, 1986; Gelles et al., 1988). The bead experiments further demonstrate that systematic drifts or positional instabilities of our apparatus are much smaller than $\sigma_r$ on the time scale of the experiments.

## ANALYSIS OF SINGLE-MOLECULE TRAJECTORIES

The lateral diffusional motion of a particle in a medium characterized by a diffusion constant $D$ is described by Fick's second law:

$$\frac{d}{dt}p(r, t) = D \cdot \nabla^2 p(r, t) \quad (1)$$

with the two-dimensional Laplacian operator, $\nabla^2$. $p(\vec{r}, t)\, d\vec{r}$ describes the probability that a particle will be detected within the area $[\vec{r}, \vec{r} + d\vec{r}]$ at a time $t$. For a particle that starts at the origin at time 0, the solution of Eq. 1 in $r^2$ yields

$$p(r^2, t)dr^2 = \left(\frac{1}{r_0^2}\right)\exp\left(-\frac{r^2}{r_0^2}\right)dr^2 \quad (2)$$

with $r_0^2(t) = 4Dt$ (Anderson et al., 1992; Almeida and Vaz, 1995). By integration, the distribution function for the square displacements $r^2$ is calculated:

$$P(r^2, t) = \int_0^{r^2} p(\rho^2, t)d\rho^2 = 1 - \exp\left(-\frac{r^2}{r_0^2}\right) \quad (3)$$

$P(r^2, t)$ is the probability that a particle starting at the origin will be found within a circle of radius $r$ at time $t$. This distribution function, which is used for the analysis of our single-molecule trajectories, is different from that of previous studies based on analysis of the mean square displacements (Geerts et al., 1987; Lee et al., 1991; Kusumi et al., 1993; Schmidt et al., 1995). The new type of analysis makes it possible to study multicomponent mobilities, as will become evident in the Results.

For each trajectory, a set of values for the square displacements, $r^2$, between two observations separated by the time lag $t_{lag}$ is obtained:

$$r^2(t_{lag}) = (\vec{r}(t + t_{lag}) - \vec{r}(t))^2 \quad (4)$$

The time lag for our experimental conditions is given by $t_{lag} = n(t_{ill} + t_{delay})$, where $t_{ill}$ is the illumination time, and $t_{delay}$ is the delay between two consecutive observations. $n$ takes on values of 1, 2, 3, . . . , $N - 1$, where $N$ denotes the total number of observations of an individual molecule ($N \leq 12$ in the POPC membrane, and $N \leq 42$ in the polymer-stabilized monolayer). For each value of $t_{lag}$, the probability $P(r^2, t_{lag})$ is constructed from multiple trajectories by counting the number of square displacements with values $\leq r^2$ normalized by the total number of data points.

## RESULTS AND DISCUSSION

### Single-molecule photon count distributions

The fluorescence photon count distributions of individually observed fluorophores are shown in the form of probability density functions in Fig. 1 for both systems studied. As pointed out in Materials and Methods, this distribution determines the positional accuracy by which a molecule can be located. Illumination times and excitation intensities were adjusted such that the same signal of a single molecule was obtained in both systems. The fluorescence photon count distribution of individual fluorescence-labeled lipids (TRITC-DHPE, *curve a*) is in excellent agreement with our previous published values (Schmidt et al., 1995). We consider this to be strong confirmation that individual molecules are being observed. The distribution is characterized by a maximum at 137 counts. Single fluorescence-labeled lipids embedded in the polymer/lipid matrix (*curve b*) are characterized by a fluorescence photon count distribution with a maximum at 159 counts. Comparison shows that the analysis of trajectories yielded similar positional accuracies, inasmuch as background noise was identical in the two systems.

It should be noted that the mean fluorescence photon counts of fluorophores embedded in the polymer/lipid matrix are shifted slightly toward higher values, although the excitation energy (illumination intensity times illumination

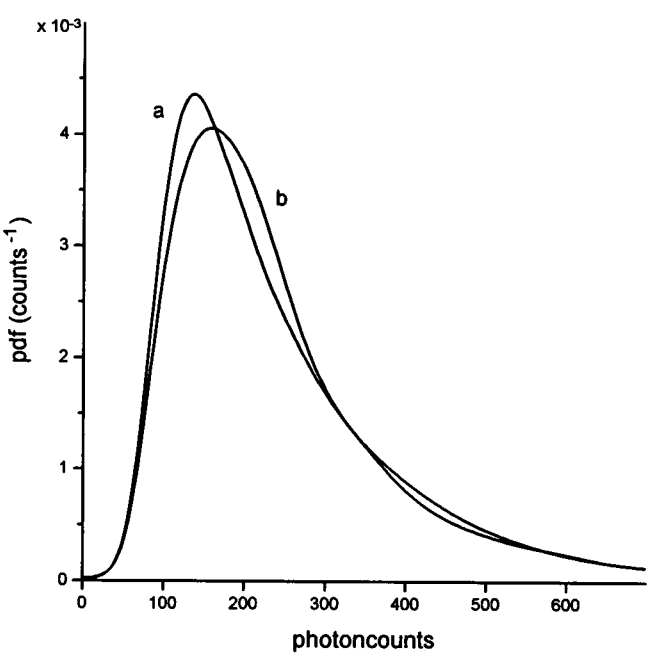


FIGURE 1 Fluorescence photon count probability distribution (pdf) calculated from 4211 individual TRITC-DHPE molecules embedded in a phospholipid membrane (*curve a*). The samples were illuminated for $t_{ill}$ = 5 ms with an intensity of 25 ± 6 kW/cm$^2$, yielding a most probable value of 137 photoncounts. Analysis of 3954 individual TRITC-DHPE molecules embedded in a polymer-stabilized phospholipid monolayer (*curve b*), illuminated for $t_{ill}$ = 1 ms with an intensity of 50 ± 12 kW/cm$^2$, yields a most probable value of 159 photoncounts.

time) was a factor of 2 less in the latter system. We attribute the increase to an increase in the fluorescence quantum yield, which strongly depends on the environment. It was reported that the fluorescence quantum yield of tetramethylrhodamine, which is 0.26 in ethanol, drops to 0.15 in water (Soper et al., 1993). The less polar environment of the polymer/lipid matrix may thus account for the higher mean fluorescence photon counts observed.

## Supported phospholipid membranes

A typical trajectory of an individual fluorescence-labeled lipid in a phospholipid membrane is shown in Fig. 2 for a time lag of 20 ms. As expected, the trajectory shows no deviation from Brownian motion; however, great care must be taken when trying to infer deviations from Brownian motion on the basis of individual trajectories (Rudnick and Gaspari, 1987; Simson et al., 1995; Saxton, 1995). An analysis of 259 trajectories yields the distribution function of the square displacements exemplified for $t_{lag} = 20$ ms in Fig. 3 *A*. The nonlinear least-squares fit (Bevington and Robinson, 1992) according to Eq. 3 (*dashed line*) obviously fails to explain the data (*closed circles*). Therefore we expanded the model by considering a fast and a slow mobility component with diffusion constants $D_1$ and $D_2$, and fractions $\alpha$ and $(1 - \alpha)$, respectively. The assumption of a two-component system also reflects results obtained in FRAP experiments in which a second component has always been observed, which is commonly interpreted as an immobile fraction. For the two-component model Eq. 3 is changed to

$$P(r^2, t) = 1 - \left[\alpha \cdot \exp\left(-\frac{r^2}{r_1^2}\right) + (1 - \alpha) \cdot \exp\left(-\frac{r^2}{r_2^2}\right)\right] \quad (5)$$

$$r_i^2(t) = 4D_i t \quad (6)$$

A least-squares fit according to Eq. 5 (Fig. 3, *solid line*) gives an excellent description of the data with no systematic deviations, as seen from the residuals. The value of the reduced $\chi_\nu^2$ decreases by two orders of magnitude for the two-component compared to the one-component model. Expansion of Eq. 5 to a model of three or more components does not significantly improve the reduced $\chi_\nu^2$ value (data not shown). The biexponential fit according to Eq. 5 yielded $r_1^2 = 0.39\ \mu m^2$, $r_2^2 = 0.036\ \mu m^2$, and $\alpha = 0.69$.

Two-component analysis was adequate for analyzing all 1317 trajectories at all delay times (15, 35, 75, and 155 ms) measured. Only data sets of at least 200 data points were included in further analysis, yielding values for $\alpha$, $r_1^2$ and $r_2^2$ as functions of $t_{lag}$ (Fig. 3, *B*, *C*, and *D*, respectively). As expected for Brownian motion, the square displacements of the first, high-mobility component, $r_1^2$, increased linearly with $t_{lag}$ (Fig. 3 *C*). The diffusion constant obtained from a linear fit according to Eq. 6 yielded $D_1 = 4.4 \pm 0.1\ \mu m^2/s$. This value is in excellent agreement with that obtained by FRAP experiments (Tamm, 1988). The second, slow-mobility component with a fraction of 25 ± 6%, constant with time lag (Fig. 3 *B*), also showed a linear increase in the square displacements for $t_{lag} > 100$ ms (Fig. 3 *D*). A linear fit yielded $D_2 = 0.072 \pm 0.002\ \mu m^2/s$.

We interpret the second, slowly mobile component as the analog of the immobile fraction observed in FRAP experiments. In the latter experiments, immobile fractions of ~25% have been observed (Tamm, 1988; Huang et al., 1992). However, from the experiments presented, it must be inferred that this fraction appears to be mobile on a small length scale of at least 300 nm, characterized by a diffusion constant ~60 times slower than that of the fast component. The discrepancy between our findings and those obtained by FRAP experiments is explained by the experimental limitations of FRAP. The lateral resolution of FRAP experiments is limited by a typical spot size of several microns. Furthermore, the dynamic range between $D_1$ and $D_2$ exceeds the properties of typical FRAP setups, being limited by the mechanical stability and signal-to-noise ratio. The finding of a two-component system here might also account for the too small diffusion constants reported for lipid motion by SPT and single-molecule imaging (Lee et al., 1991; Anderson et al., 1992; Schmidt et al., 1995) when compared to FRAP experiments (Tamm, 1988). In those SPT experiments, in contrast to the distribution analysis used here, the mean square displacement was analyzed, which resulted in an averaged lateral diffusion constant over both the fast and slow components.

For $t_{lag} < 100$ ms, the second component was constant ($r_2^2 = 0.030 \pm 0.006\ \mu m^2$). This value is above the mini-

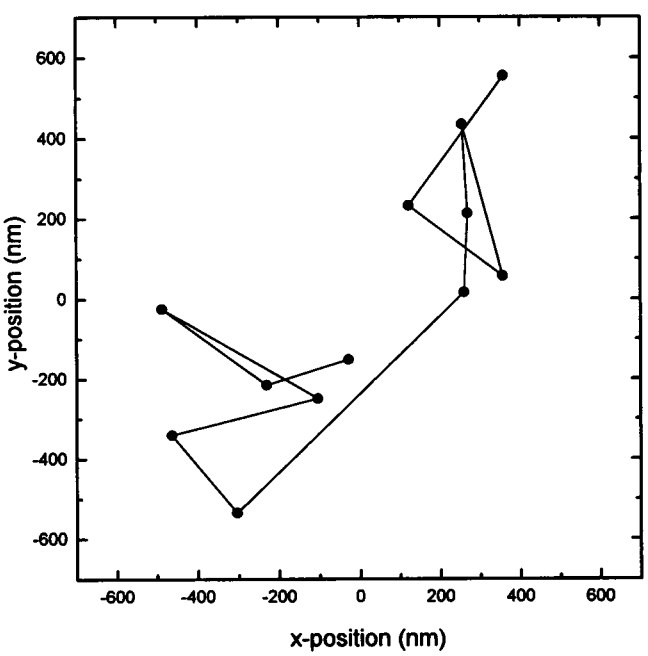


FIGURE 2 Trajectory of a single TRITC-DHPE molecule embedded in a fluid phospholipid membrane. The time lag between two consecutive observations was 20 ms.

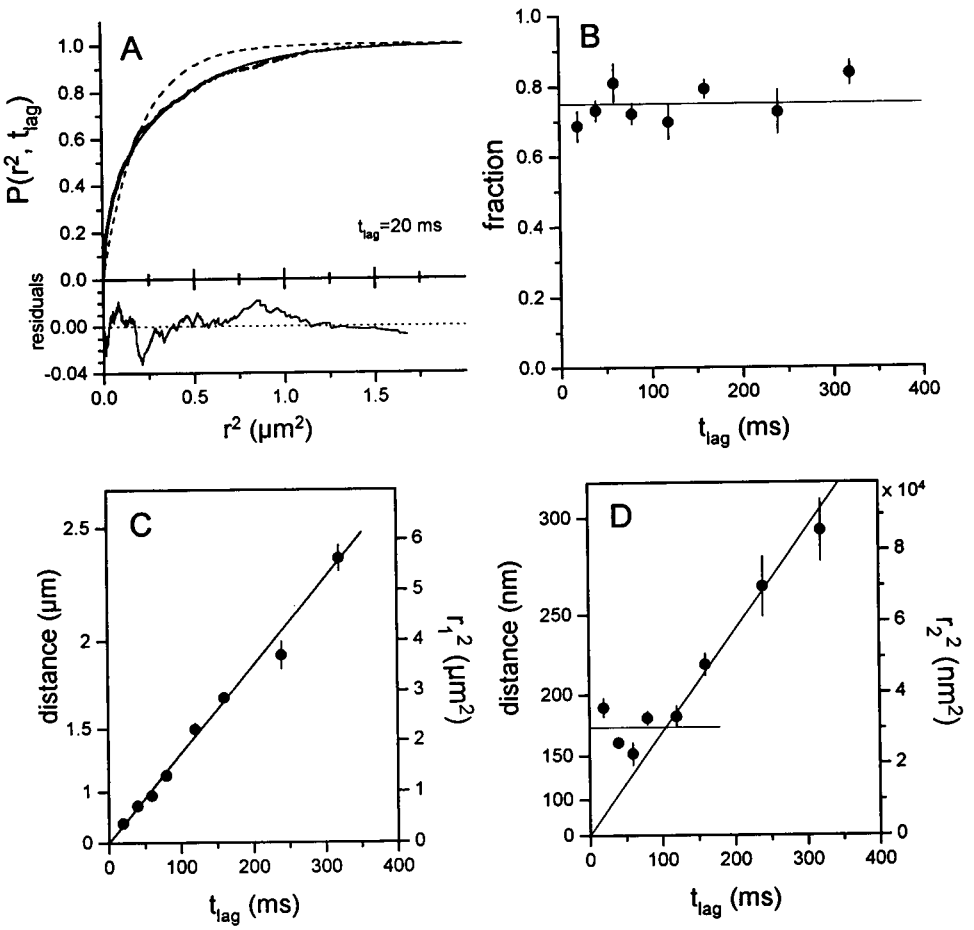


FIGURE 3 (*A*) Distribution function for square displacements, $P(r^2,t_{lag})$, of individual TRITC-DHPE molecules in a fluid phospholipid membrane at $t_{lag}$ = 20 ms. A total of 259 trajectories are included in this analysis, yielding 571 data points (●). The solid line represents the result of a fit according to Eq. 5, yielding $r_1^2$ = 0.39 ± 0.02 μm², $r_2^2$ = 0.036 ± 0.003 μm², and $\alpha$ = 0.69 ± 0.04. The residuals show no systematic deviation of the fit from the data. The fit according to Eq. 3 (– – –) fails. (*B*) The fraction of the fast component is constant between 20 ms and 320 ms, and is characterized by a mean of 0.75 ± 0.06 (——). (*C*) Expectation value for the square displacements of the fast component, $r_1^2$ (*right axis*), plotted versus $t_{lag}$. A linear fit according to Eq. 6 yields $D_1$ = 4.4 ± 0.1 μm²/s (——). (*D*) The expectation value for the square displacements of the slow component, $r_2^2$ (*right axis*), increases linearly with $t_{lag}$ for $t_{lag}$ > 100 ms, yielding a diffusion constant $D_2$ = 0.072 ± 0.002 μm²/s. For $t_{lag}$ < 100 ms, $r_2^2$ is constant, with a mean value of 0.030 ± 0.006 μm². Note that the highest value of $r_2^2$ measured reflects a displacement of <300 nm (*left axis*). (*C* and *D*) Error bars for each $r_i^2$ are given by $r_i^2/\sqrt{N}$, with *N* denoting the number of independent data points in *A*, determined according to the method of Quian et al. (1991).

mum detectable square displacement of $108^2$ nm² = 0.012 μm². We interpret this constant value to be caused by lateral restrictions of the mobility in the range of 100 nm. Monte Carlo simulations for lateral diffusion restricted to square corrals were performed (not shown), yielding a monoexponential increase in $P(r^2, t)$ on $r^2$ according to Eq. 3. In contrast to free Brownian motion, $r_0^2(t_{lag})$ converges to $R^2$ for large $t_{lag}$, where $R$ is the typical size of the corral (Saxton, 1993). Taking into account the minimum square displacement given by the signal-to-noise ratio of $108^2$ nm², the constant value for $t_{lag}$ < 100 ms reflects restrictions for lateral diffusion of $\sqrt{3.0 \times 10^4 - 108^2\, nm^2}$ ~130 nm. Monte Carlo simulations further show that a fast increase in $r_2^2$ should be observed (see also Saxton, 1993). To resolve the initial increase, however, a time resolution of <2 ms would be required, which cannot be accomplished by our experimental setup at present. The region of the transition between confined diffusion and slow, unrestricted diffusion at ~100 ms is characterized by small systematic deviations in the biexponential fit from the data (not shown). Distributions for $t_{lag}$ = 80 and 120 ms were fitted according to a three-component model that slightly reduced the value of $\chi_\nu^2$, but the solutions were numerically unstable. All findings can be understood by the assumption that the second component splits into two parts: one part resembles strictly confined diffusion within a corral of ~130 nm; the second part comprises molecules that have left the corral within $t_{lag}$.

## Polymer-stabilized phospholipid monolayer

Poly(methacrylate) (PMA) stabilized POPC monolayers with a lipid content of 5% (w/w) were deposited on phospholipid-monolayer-coated glass substrates at a surface pressure of 20 mN/m, as described in Materials and Methods. Under these conditions, photobleaching experiments using unpolarized light have been performed (Kowack and Helm, 1995) that showed no lateral mobility on length scales larger than 10 μm. When polarized light was used in these experiments, however, strong evidence for the rotational mobility of the fluorophores was found (C. A. Helm, personal communication). It was suggested that lateral mobility on length scales smaller than 10 μm should be observable. The lipid phase is expected to be incorporated into voids of the polymer matrix, which forms restrictions or corrals for the lateral mobility of the phospholipids. In the following, experimental evidence for this model and an estimation for the average corral size are given.

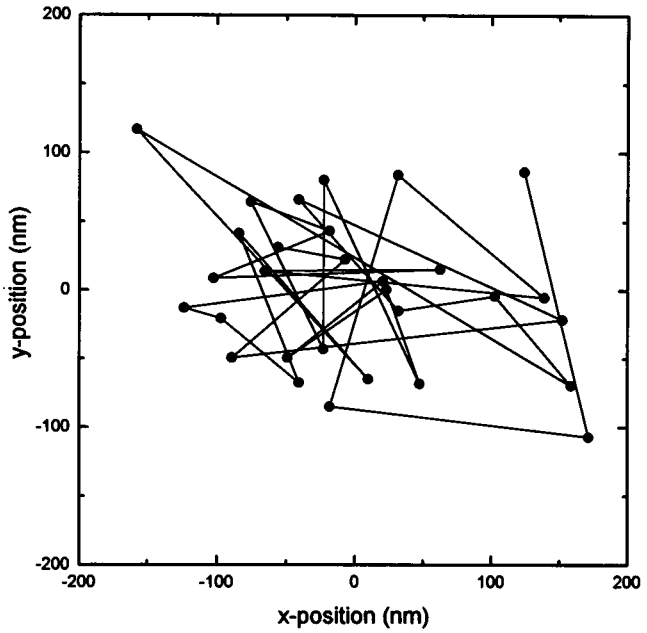


FIGURE 4 Trajectory of an individual TRITC-DHPE molecule embedded in a polymer-stabilized phospholipid monolayer. The time lag between two observations was 3.2 ms.

Fig. 4 shows a typical trajectory of an individual fluorescence-labeled phospholipid in the polymer matrix for $t_{lag}$ = 3.2 ms. In comparison to the trajectory shown in Fig. 2, mobility of the molecule in the polymer matrix appears to be restricted to an area ~200 nm in diameter.

Averaging 896 trajectories yields the distribution function for the square displacements shown in Fig. 5 *A* for $t_{lag}$ = 3.2 ms. Similar to the supported phospholipid membrane, all data follow a biexponential increase according to Eq. 5, which is indicative of a two-component system. For the data shown in Fig. 5 *A*, the least-squares fit yielded $r_1^2$ = 3.7 × $10^4$ nm$^2$, $r_2^2$ = 9.5 × $10^3$ nm$^2$, and $\alpha$ = 0.39. All data sets between $t_{lag}$ = 3.2 and 44.8 ms were fit accordingly. No variation of the fit parameter $\alpha$, $r_1^2$, and $r_2^2$ was detected over the entire range of $t_{lag}$ (Fig. 5, *B–D*), yielding average values of $\alpha$ = 0.45 ± 0.11, $r_1^2$ = 3.2 ± 0.6 × $10^4$ nm$^2$, and $r_1^2$ = 8.1 ± 1.4 × $10^3$ nm$^2$.

These results are expected for the corralled diffusion model proposed. As discussed in the previous section, diffusion in a restricted area yields a constant square displacement with time lag, where the mean of the square displacements reflects the average size of that confinement area. The first component, characterized by $r_1^2$, exhibits a corral size of

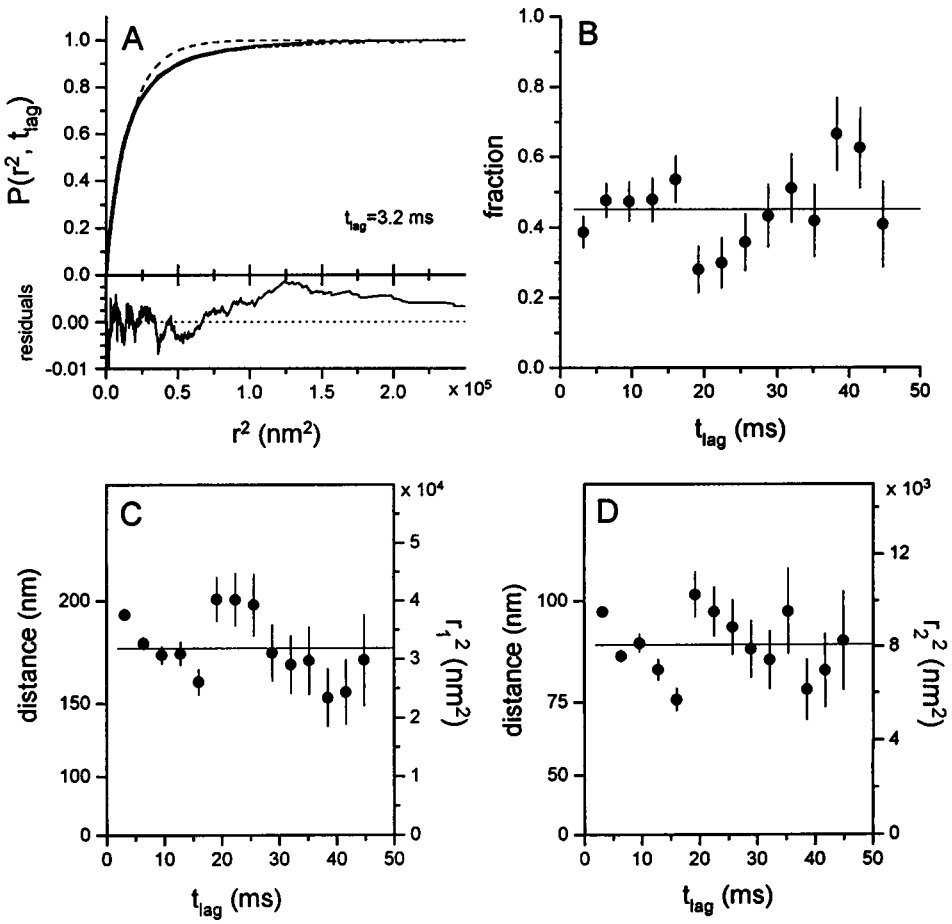


FIGURE 5 (*A*) Distribution function for the square displacements, $P(r^2,t_{lag})$, of individual TRITC-DHPE molecules in a polymer-stabilized phospholipid monolayer. The analysis includes 896 trajectories, yielding 2494 data points (●). The solid line shows a fit according to Eq. 5, yielding $r_1^2$ = 3.7 ± 0.1 × $10^4$ nm$^2$, $r_2^2$ = 9520 ± 241 *nm*$^2$, and $\alpha$ = 0.39 ± 0.04. (*B*) The fraction of the large component is constant between 3.2 and 48 ms, with a mean value of 0.45 ± 0.11 (——). (*C*) The expectation value for square displacements of the large component, $r_1^2$ (*right axis*), is constant, with a mean value of 3.2 ± 0.6 × $10^4$ nm$^2$ (——), corresponding to a typical distance of 178 nm (*left axis*). (*D*) The expectation value for the square displacements of the small component, $r_2^2$, is constant, with a mean value of 8.1 ± 1.4 × $10^3$ nm$^2$, reflecting the accuracy of the distance determination (——). (*C* and *D*) Error bars are determined as in Fig. 3.

$\sqrt{3.2 \times 10^4 - 108^2\, nm^2} \sim 140$ nm on average when the limited accuracy of 108 nm for distance determinations is taken into account. Our current time resolution does not permit us to resolve the initial increase of $r_1^2$ with $t_{lag}$, which would require experiments on a time scale of 800 $\mu$s when a diffusion constant of 4.4 $\mu m^2/s$ is assumed. The second component, reflecting about half of all molecules, exhibits lateral shifts at the detection limit; thus it is not discernible whether they are immobile or mobile on length scales below 100 nm. These findings demonstrate that at least half of the lipid molecules in such a polymer-stabilized monolayer are mobile on typical length scales of 140 nm.

## CONCLUSIONS

We have presented an alternative method for analyzing SPT and single-molecule tracking data based on the construction of the probability distribution of the square displacements. The main advantage of the described methodology is its ability to access parameters such as individual diffusion constants and fractions of multiple-component samples, which are inaccessible in standard ensemble averaging studies. Although our data analysis still relies on ensemble averaging, it has the capability of discerning between at least two classes of mobility. In principle, data on individual molecules would permit analysis of single trajectories. However, as has been pointed out by various authors (Saxton, 1995; Simson et al., 1995), such diffusion analysis using individual trajectories of relatively small length is not straightforward. It will be a challenging task for the future to develop an appropriate methodology for the analysis of such individual trajectories.

Analysis of single-molecule trajectories in two systems, a supported phospholipid membrane in the fluid state and a polymer-stabilized phospholipid monolayer, clearly revealed deviations from free Brownian motion on a lateral scale of 100 nm. The two components of the phospholipid membrane are identified with the mobile and immobile fraction commonly found in FRAP experiments. These examples demonstrate that probability distribution analysis, in combination with ultrasensitive single-molecule imaging techniques, might have the potential to reveal details of lateral mobility in biological membranes. In particular, the high lateral accuracy of these methods provides an alternative tool for the study of dynamics and lateral organization on the plasma membrane, with the ability to test different models.

We acknowledge P. Hinterdorfer for the stimulating discussions on mobility in phospholipid membranes, W. Baumgartner for elucidating comments on statistical data analysis, C. Helm for providing us with the PMA samples, and H. Gruber for his assistance in sample preparation.

The Austrian Research Fond is acknowledged for financial support (project S06607-MED).

## REFERENCES

Almeida, P. F. F., and W. L. C. Vaz. 1995. Lateral diffusion in membranes. *In* Handbook of Biological Physics, Vol. 1. R. Lipowsky and E. Sackmann, editors. Elsevier/North Holland, Amsterdam. 305–357.

Anderson, C. M., G. N. Georgiou, I. E. G. Morrison, G. V. W. Stevenson, and R. J. Cherry. 1992. Tracking of cell surface receptors by fluorescence digital imaging microscopy using a charge-coupled device camera. *J. Cell Sci.* 101:415–425.

Axelrod, D., D. E. Koppel, J. Schlessinger, E. Elson, and W. W. Webb. 1976. Mobility measurement by analysis of fluorescence photobleaching recovery kinetics. *Biophys. J.* 16:1055–1069.

Bevington, P. R., and D. K. Robinson. 1992. Data Reduction and Error Analysis for the Physical Sciences. McGraw-Hill, New York.

Bobroff, N. 1986. Position measurement with a resolution and noise-limited instrument. *Rev. Sci. Instrum.* 57:1152–1157.

Edidin, M. 1992. Translational diffusion of membrane proteins. *In* The Structure of Biological Membranes. P. Yeagle, editor. CRC Press, Boca Raton, FL. 539–572.

Edidin, M., S. C. Kuo, and M. P. Sheetz. 1991. Lateral movements of membrane glycoproteins restricted by dynamic cytoplasmic barriers. *Science.* 254:1379–1382.

Feder, T. J., I. Brust-Mascher, J. P. Slattery, B. Baird, and W. W. Webb. 1996. Constrained diffusion or immbile fraction on cell surfaces: a new interpretation. *Biophys. J.* 70:2767–2773.

Funatsu, T., Y. Harada, M. Tokunaga, K. Saito, and T. Yanagida. 1995. Imaging of single fluorescent molecules and individual ATP turnovers by single myosin molecules in aqueous solution. *Nature.* 374:555–559.

Geerts, H., M. De Brabander, R. Nuydens, S. Geuens, M. Moermans, J. De Mey, and P. Hollenbeck. 1987. Nanovid tracking: a new automatic method for the study of mobility in living cells based on colloidal gold and video microscopy. *Biophys. J.* 52:775–782.

Gelles, J., B. J. Schnapp, and M. P. Sheetz. 1988. Tracking kinesin-driven movements with nanometre-scale precision. *Nature.* 331:450–453.

Ghosh, R. N., and W. W. Webb. 1994. Automated detection and tracking of individual and clustered cell surface low density lipoprotein receptor molecules. *Biophys. J.* 66:1301–1318.

Gross, D., and W. W. Webb. 1986. Molecular counting of low-density lipoprotein particles as individuals and small clusters on cell surfaces. *Biophys. J.* 49:901–911

Huang, Z., K. H. Pearce, and N. L. Thompson. 1992. Effect of bovine prothrombin fragment 1 on the translational diffusion of phospholipids in Langmuir-Blodgett monolayers. *Biochim. Biophys. Acta.* 1112: 259–265.

Jacobson, K., E. D. Sheets, and R. Simson. 1995. Revisiting the fluid mosaic model of membranes. *Science.* 268:1441–1442.

Kalb, E., S. Frey, and L. K. Tamm. 1992. Formation of supported planar bilayers by fusion of vesicles to supported phospholipid monolayers. *Biochim. Biophys. Acta.* 1103:307–316.

Kowack, K., and C. A. Helm. 1995. Immobilization of functionalized lipids in a random poly(methacrylate) copolymer monolayer. *Adv. Mater.* 7:156–160.

Kubitschek, U., P. Wedekind, and R. Peters. 1994. Lateral diffusion measurement at high spatial resolution by scanning microphotolysis in a confocal microscope. *Biophys. J.* 67:948–956.

Kusumi, A., Y. Sako, and M. Yamamoto. 1993. Confined lateral diffusion of membrane receptors as studied by single particle tracking (Nanovid microscopy). Effects of calcium-induced differentiation in cultured epithelial cells. *Biophys. J.* 65:2021–2040.

Lee, G. M., A. Ishihara, and K. A. Jacobson. 1991. Direct observation of Brownian motion of lipids in a membrane. *Proc. Natl. Acad. Sci. USA.* 88:6274–6278.

Peters, R. 1988. Lateral mobility of proteins and lipids in the red cell membrane and the activation of adenylate cyclase by beta-adrenergic receptors. *FEBS Lett.* 234:1–7.

Quian, H., M. P. Sheetz, and E. L. Elson. 1991. Single particle tracking: analysis of diffusion and flow in two-dimensional systems. *Biophys. J.* 60:910–921.

Rudnick, J., and G. Gaspari. 1987. The shapes of random walks. *Science.* 237:384–389.

Saffman, P. G., and M. Delbrück. 1975. Brownian motion in biological membranes. *Proc. Natl. Acad. Sci. USA.* 72:3111–3113.

Sako, Y., and A. Kusumi. 1995. Barriers for lateral diffusion of transferrin receptor in the plasma membrane as characterized by receptor dragging by laser tweezers: fence versus tether. *J. Cell Biol.* 129:1559–1574.

Sase, I., H. Miyata, J. E. T. Corrie, J. S. Craik, and K. Kinosita, Jr. 1995. Real time imaging of single fluorophores on moving actin with an epifluorescence microscope. *Biophys. J.* 69:323–328.

Saxton, M. J. 1993. Lateral diffusion in an archipelago: single-particle diffusion. *Biophys. J.* 64:1766–1780.

Saxton, M. J. 1994. Single-particle tracking: models of directed transport. *Biophys. J.* 67:2110–2119.

Saxton, M. J. 1995. Single-particle tracking: effects of corrals. *Biophys. J.* 69:389–398.

Schmidt, Th., G. J. Schütz, W. Baumgartner, H. J. Gruber, and H. Schindler. 1995. Characterization of photophysics and mobility of single molecules in a fluid lipid membrane. *J. Phys. Chem.* 99:17662–17668.

Schmidt, Th., G. J. Schütz, W. Baumgartner, H. J. Gruber, and H. Schindler. 1996. Imaging of single molecule diffusion. *Proc. Natl. Acad. Sci. USA.* 93:2926–2929.

Sheetz, M. P., M. Schindler, and D. E. Koppel. 1980. Lateral mobility of integral membrane proteins is increased in spherocytic erythrocytes. *Nature.* 285:510–512.

Simson, R., E. D. Sheets, and K. Jacobson. 1995. Detection of temporary lateral confinement of membrane proteins using single-particle tracking analysis. *Biophys. J.* 69:989–993.

Singer, S. J., and G. L. Nicholson. 1972. The fluid mosaic model of the structure of cell membranes. *Science.* 175:720–731.

Soper, S. A., H. L. Nutter, R. A. Keller, L. M. Davis, and E. B. Shera. 1993. The photophysical constants of several fluorescent dyes pertaining to ultrasensitive fluorescence spectroscopy. *Photochem. Photobiol.* 57: 972–977.

Tamm, L. K. 1988. Lateral diffusion and fluorescence microscope studies on a monoclonal antibody specifically bound to supported phospholipid bilayers. *Biochemistry.* 27:1450–1457.

Tocanne, J. F. 1992. Detection of lipid domains in biological membranes. *Comments Mol. Cell. Biophys.* 8:53–72.

Zhang, F. G., G. M. Lee, and K. Jacobson. 1993. Protein lateral mobility as a reflection of membrane microstructure. *BioEssays.* 15:579–588.